# Robust High-κ Response in Molecularly Thin Perovskite Nanosheets

**Minoru Osada,[†,‡,*] Kosho Akatsuka,[†,‡] Yasuo Ebina,[†,‡] Hiroshi Funakubo,[§] Kanta Ono,[⊥] Kazunori Takada,[†,‡] and Takayoshi Sasaki[†,‡]**

[†]International Center for Materials Nanoarchitectonics (MANA), National Institute for Materials Science, Tsukuba, Ibaraki 305-0044, Japan, [‡]CREST, Japan Science and Technology Agency, Kawaguchi, Saitama 332-0012, Japan, [§]Department of Innovative and Engineered Materials, Tokyo Institute of Technology, Yokohama 226-8502, Japan, and [⊥]Institute of Materials Structure Science, High Energy Accelerator Research Organization, Tsukuba, Ibaraki 305-0801, Japan

**ABSTRACT** Size-induced suppression of permittivity in perovskite thin films is a fundamental problem that has remained unresolved for decades. This size-effect issue becomes increasingly important due to the integration of perovskite nanofilms into high-κ capacitors, as well as concerns that intrinsic size effects may limit their device performance. Here, we report a new approach to produce robust high-κ nanodielectrics using perovskite nanosheet ($Ca_2Nb_3O_{10}$), a new class of nanomaterials that is derived from layered compounds by exfoliation. By a solution-based bottom-up approach using perovskite nanosheets, we have successfully fabricated multilayer nanofilms directly on $SrRuO_3$ or Pt substrates without any interfacial dead layers. These nanofilms exhibit high dielectric constant (>200), the largest value seen so far in perovskite films with a thickness down to 10 nm. Furthermore, the superior high-κ properties are a size-effect-free characteristic with low leakage current density ($<10^{-7}$ A cm$^{-2}$). Our work provides a key for understanding the size effect and also represents a step toward a bottom-up paradigm for future high-κ devices.

**KEYWORDS:** perovskite nanosheets · layer-by-layer assembly · high-κ dielectrics · size effect

The ever-increasing requirements on miniaturization and efficiency of electronic components result in efforts to incorporate new nanomaterials into microelectronics, in order to overcome the physical limits of current materials. In the case of a specific class of materials, high-κ dielectric oxides, this challenge is particularly topical. High-κ oxides find various applications in a remarkably broad spectrum of advanced electronic components such as dynamic random access memories, embedded capacitors, tunable devices, energy storage, gate dielectrics, *etc.*[1−4] In this context, the most recent International Technology Roadmap for Semiconductors (ITRS) predicts the implementation of high-κ ultrathin films (<10 nm) in future applications.[5]

Capacitor components based on dielectric thin films are the largest elements in integrated circuits, and reducing their size and increasing their speed is an important step in the advancement of electronics. Central to these researches is the design and integration of new high-κ oxides that afford robust high-κ properties even at several nanometer thicknesses, allowing high capacitances with acceptably low leakage currents.[4,6] Extensive efforts have thus been directed at reducing their size through the use of perovskite oxides such as $SrTiO_3$ and $(Ba_{1-x}Sr_x)TiO_3$. However, perovskite thin films often yield reduced dielectric constants that are 1 order of magnitude smaller than bulk values.[7−13] This so-called "size effect" is a long-standing conundrum in perovskites, which severely limits their device performance.[14−17]

The size effect is often discussed in terms of a low-κ interfacial dead layer.[18−21] At present, two models have been used to describe the dead layer, namely of extrinsic and intrinsic origins. The extrinsic origins claimed in literature are the degradation of a film/electrode interface and the strains imposed by electrodes.[13] The incomplete screening of dipole charges by electrodes is rather regarded as the intrinsic origin.[12,18,19,21] However, the situation is even more complicated in actual systems. Current film growth techniques require complex deposition processes with high-temperature postannealing (>600 °C), producing large extrinsic effects arising from growth-induced defects and thermal strain. Thus, a key challenge in this field is the production of dead-layer-free nanofilms by engineering the dielectric/electrode interface at the atomic scale, which may realize the full potential of high-κ perovskites.

Herein, we demonstrate the experimental realization of such an ideal nanofilm, in which we control the dielectric/electrode interface by solution-based room-temperature fabrication using perovskite nanosheet ($Ca_2Nb_3O_{10}$) as a building block.

*Address correspondence to osada.minoru@nims.go.jp.

Received for review June 27, 2010 and accepted August 05, 2010.

**Published online August 24, 2010.**
**10.1021/nn101453v**

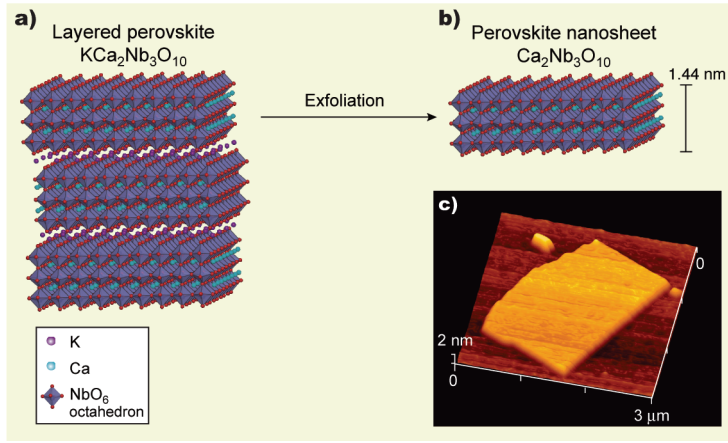


**Figure 1. A process flow of perovskite nanosheets. (a) Structure of the starting layered perovskite $KCa_2Nb_3O_{10}$. The layered host material undergoes exfoliation upon interacting with $TBA^+$ ions, and a colloidal suspension of unilamellar perovskite nanosheets is thus obtained. (b) Structure of $Ca_2Nb_3O_{10}$ perovskite nanosheet. The nanosheet consists only of $NbO_6$ octahedra, a key building block of perovskite dielectrics. (c) Typical AFM image of individual $Ca_2Nb_3O_{10}$ nanosheet deposited onto a Si substrate. Its thickness is ~1.8 ± 0.1 nm, being comparable to the crystallographic thickness (1.44 nm) of the host layer in the starting material ($KCa_2Nb_3O_{10}$).**

Perovskite nanosheets investigated here are a new class of nanomaterials that are derived from layered perovskites by exfoliation (Figure 1).[22,23] The exfoliated nanosheets are characterized by a two-dimensional (2D) single crystal with a molecular thickness; the thickness is only ~1.4 nm, corresponding to three $NbO_6$ octahedral nanoblocks. These nanosheets consist only of $NbO_6$ octahedral nanoblocks susceptible to a large molecular polarizability, which makes the nanosheet an ideal base for high-κ dielectrics with the critical thickness. The molecular polarizability (α), in particular the dipole polarizability that arises from the structure, is a key parameter for the permittivity (κ) of a material; these two quantities are linked through the Clausius−Mossotti relation [$\kappa = (1 + 8\pi\alpha_m/3V_m)/(1 - 4\pi\alpha_m/3V_m)$] where $V_m$ is the molar volume.[24] In bulk systems such as perovskite oxides, a variety of strategies has been put forth for designing new high-κ dielectrics through the substitution of more polarizable ions into the lattice. Such a materials design in low-dimensional nanomaterials is a challenge, but a large increase in κ could be achieved by increasing dipole polarizability and decreasing molar volumes of nanosheets. We here show that such a materials design can be achieved by perovskite nanosheets. The layer-by-layer assembled multilayer films on $SrRuO_3$ or Pt substrates enhance the permittivity (>200) and simultaneously stabilize its dielectric response in the ultrathin form (<10 nm), contrasting to typical perovskite films.

## RESULTS AND DISCUSSION

A colloidal suspension of perovskite nanosheet ($Ca_2Nb_3O_{10}$) with the lateral dimension of *ca.* 3−10 μm was prepared by delaminating layered perovskite ($KCa_2Nb_3O_{10}$) according to previously described procedures.[22,23] We approached the preparation of multilayered nanodielectrics by a layer-by-layer assembly using the Langmuir−Blodgett (LB) process (Figure 2a, see Methods).[25,26] This LB approach with the use of an atomically flat $SrRuO_3$ substrate is effective for the fabrication of an atomically uniform monolayer film with a highly dense characteristic. Repeated LB deposition of the monolayer could yield multilayer $(Ca_2Nb_3O_{10})_n$ nanofilms (Figures 2a,b). The as-deposited $(Ca_2Nb_3O_{10})_n$ films were irradiated by ultraviolet light (UV) in order to decompose tetrabutylammonium ($TBA^+$) ions used in the exfoliation process. The final product was identified as an inorganic multilayer assembly accommodating $NH_4^+$ ions as a consequence of total photocatalytic removal of $TBA^+$ ions.

We fabricated multilayer $(Ca_2Nb_3O_{10})_n$ nanofilms with film thicknesses ranging between 4.5 and 22.5 nm. Here, the film thickness was calibrated using the intersheet spacing (1.5 nm) determined by high-resolution transmission electron microscopy (HRTEM) and X-ray diffraction (XRD). An atomic force microscopy (AFM) image (Figure 2c) revealed that $(Ca_2Nb_3O_{10})_n$ ($n = 3$) film appeared flat on the atomic scale and uniform over a large area; the roughness (root-mean-square) was ~0.3 nm. These nearly perfect characteristics persist in monolayer and thicker films, indicating that the high-quality monolayer could be repeatedly deposited to yield a well-ordered lamellar structure in multilayer films. Cross-sectional TEM image of the $(Ca_2Nb_3O_{10})_n$ ($n = 3$) film (Figure 2d) revealed that the substrate surface is covered with the multilayer film, and the coverage and film thickness are homogeneous in a wide area.

Figure 3 depicts the XRD pattern for the $(Ca_2Nb_3O_{10})_n$ ($n = 10$) film fabricated on the quartz glass. The film showed the 00*l* basal reflections up to the eighth order line, indicating high structural order. The basal series can be ascribed to the stacked structure of the nanosheets with an interlayer distance of 1.50 nm.

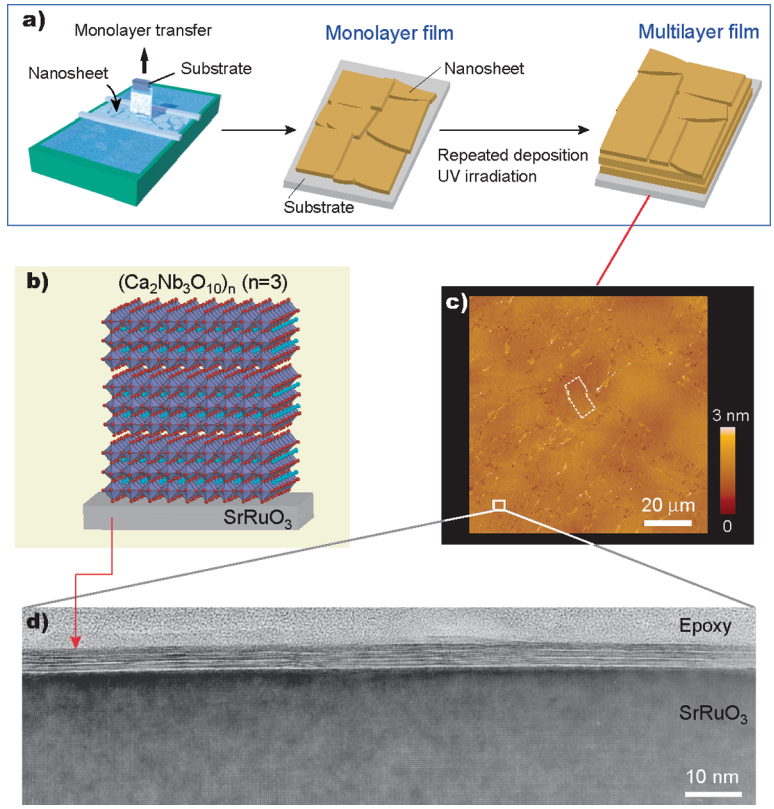


**Figure 2. (a) Fabrication procedure for multilayer films using the LB method. (b) Schematic representation of layer-by-layer assembly of perovskite nanosheets. (c) AFM image of a $(Ca_2Nb_3O_{10})_n$ ($n$ = 3) film on a $SrRuO_3$ substrate. This image clearly visualizes the adsorbed nanosheets, which give an efficient surface coverage (~100%) on the substrate surface as a consequence of the controlled packing density in the LB process. (d) Cross-sectional HRTEM image of a $(Ca_2Nb_3O_{10})_n$ ($n$ = 3) film on a $SrRuO_3$ substrate.**

Cross-sectional HRTEM observations provide direct information on the multilayer structure. Figure 4 shows higher magnification HRTEM images of the $(Ca_2Nb_3O_{10})_n$ ($n$ = 3, 5, 10) films. The regular growth structure composed of $Ca_2Nb_3O_{10}$ layers is clearly seen. The thicknesses of the constituent layers were approximately 1.5 nm, which are in good agreement with the crystallographic thicknesses (1.44 nm) of $Ca_2Nb_3O_{10}$ nanosheets and the interlayer distance (1.50 nm) in XRD data. In addition, there are no detectable stacking defects in the film. These results clearly indicate that the well-ordered lamellar structure of $Ca_2Nb_3O_{10}$ nanosheets is maintained not only in nanometer scale but also in a wider-ranging area.

Electron energy-loss spectroscopy (EELS) in TEM was used to probe compositional changes at the interface (Figure 5). Simultaneously recorded O-*K* and Ca-*L* edge spectra show a compositional abruptness between $SrRuO_3$ substrate and subsequently deposited nanosheets; a comparison with reference O-*K* edge spectra from $KCa_2Nb_3O_{10}$ and $SrRuO_3$ indicates that the lamellar parts (points 1−4) are composed of $Ca_2Nb_3O_{10}$. At the interface (Point 5), the main features in the O-*K* spectrum closely match those of $SrRuO_3$. We note that there are no detectable interdiffusion and strains at the interface, suggesting the production of a dead-layer-free perovskite nanofilms directly assembled on the $SrRuO_3$ substrate. Such a superior interface property is not specific to the materials choice and interface geometry; the multilayer films of a similar quality were achieved in $(Ca_2Nb_3O_{10})_n$ with different stackings ($n$) and different substrates such as Pt or $SrTiO_3$:Nb (Figure 4, Figure S1, Supporting Information). Therefore, we may conclude that the exact control of interface atomic stackings can be realized in the self-assembled nanofilms.

Such well-organized multilayer films lead to remarkable dielectric properties even for thicknesses as small as 5 nm. Leakage current and dielectric properties were investigated by making Au/$(Ca_2Nb_3O_{10})_n$/$SrRuO_3$ capacitors. Figure 6 shows leakage current density *versus* volt-

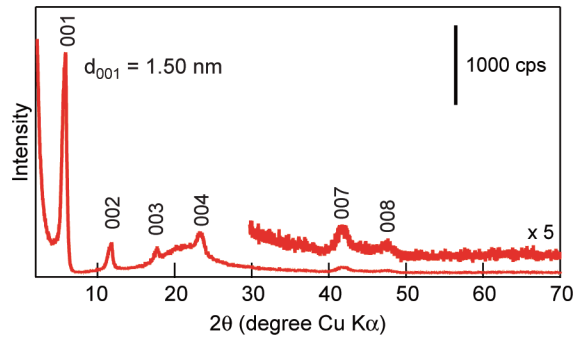


**Figure 3. XRD pattern for the $(Ca_2Nb_3O_{10})_n$ ($n$ = 10) film fabricated on a quartz glass.**

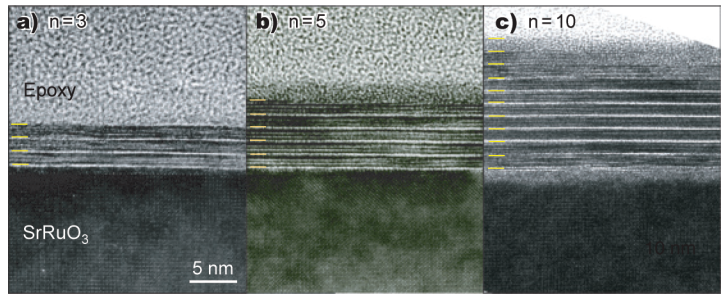


**Figure 4. High magnification HRTEM images of the $(Ca_2Nb_3O_{10})_n$ ($n$ = 3, 5, 10) films on $SrRuO_3$ substrate. The lines are a guide for the layer stackings.**

age ($J-V$) curves of multilayer $(Ca_2Nb_3O_{10})_n$ films with different thicknesses. A 4.5-nm-thick $(Ca_2Nb_3O_{10})_n$ film ($n$ = 3) shows excellent insulating characteristics, giving a leakage current density of $\sim 10^{-7}$ A cm$^{-2}$ at +1 V. Even lower $J$ values are obtained for thicker films composed of 5-, 10-, and 15-layered nanosheets. These $J$ values are much lower, at least 2 orders of magnitude lower than the performance of comparable films of $(Ba_{1-x}Sr_x)TiO_3$.[7] These $(Ca_2Nb_3O_{10})_n$ films also exhibit strong dielectric endurance in a high electrical field; dielectric breakdown occurs at ~3.4 MV cm$^{-1}$ in the 4.5-nm-thick film.

In Figure 7, we show the frequency dependence of the relative dielectric constant ($\varepsilon_r$) in a 7.5-nm-thick $(Ca_2Nb_3O_{10})_n$ ($n$ = 5) film together with the data of bulk $KCa_2Nb_3O_{10}$. The observed $\varepsilon_r$ values (~210) of $Ca_2Nb_3O_{10}$ nanosheets are high even in the ultrathin geometry (<10 nm), which attains the bulk $\varepsilon_r$ value (~230 at 100 kHz) of $KCa_2Nb_3O_{10}$. The $\varepsilon_r$ values exhibit a rather flat frequency dispersion within 5% in the regime of 1 kHz−10 MHz, contrasting to that of bulk $KCa_2Nb_3O_{10}$ and $HCa_2Nb_3O_{10}$ ceramics[27,28] where high-frequency $\varepsilon_r$ values are depleted possibly due to the charge separation and/or the dielectric relaxation of included water.

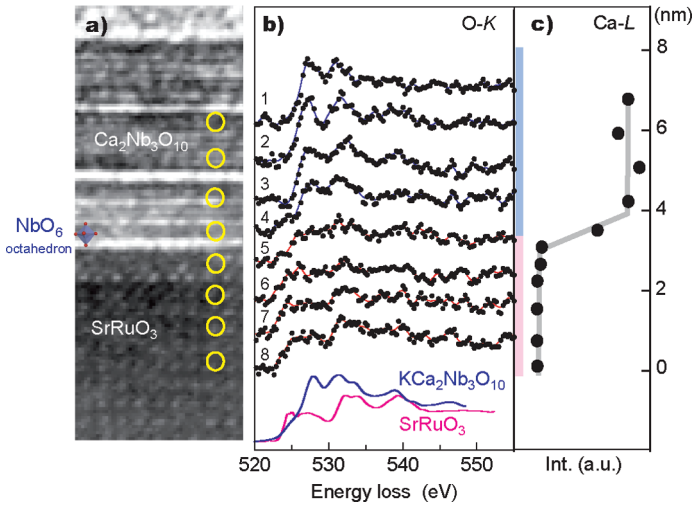


**Figure 5. (a) HRTEM image, (b) O-$K$ edge EELS profile, and (c) integrated intensity profile of the Ca-$L$ edge EELS across a $(Ca_2Nb_3O_{10})_n/SrRuO_3$ ($n$ = 3) film. The electron beam position for these data is denoted by circles in the HRTEM image as well as numbers in the O-$K$ edge spectra. In the HRTEM image, the three equidistant dark fringes in $Ca_2Nb_3O_{10}$ represent elementary units of $NbO_6$ octahedral layers.**

In addition, these superior insulating and dielectric properties are independent of the probe area and electrode sizes. To check the possible effects of the lateral size and nanosheet edges on dielectrics properties, we also carried out experiments on various capacitors (with different size electrodes of 10 × 10, 50 × 50, and 100 × 100 μm$^2$), and obtained almost identical results (with the standard deviations of ±5%) even using the different size electrodes. These results again indicate good homogeneity of the multilayer films, and there is no significant effect of the lateral size and nanosheet edges in our nanosheet capacitors.

Figure 8a shows the variation of $\varepsilon_r$ in the multilayer $(Ca_2Nb_3O_{10})_n$ films as a function of the film thickness. The $\varepsilon_r$ values of these films keep a constant level of ~210 irrespective of the film thickness where the dielectric loss tan δ is around 2−5%. Figure 8b is the thickness dependence of the reciprocal capacitance $1/C$ for the $(Ca_2Nb_3O_{10})_n$ films. In $(Ba_{1-x}Sr_x)TiO_3$, there exists a nonzero $1/C$ intercept, due to the presence of a certain interfacial low-κ dead layer.[9,12] In contrast, the $(Ca_2Nb_3O_{10})_n$ films show a linear relationship across the zero. The estimated $\varepsilon_r$ from the $1/C$ slope is ~210, compatible with the measured $\varepsilon_r$ value in Figure 8a. These results indicate the absence of an interfacial dead layer inside the films.

Such a superior dielectric property is not specific to $Ca_2Nb_3O_{10}$ nanosheet; a simultaneous improvement of $\varepsilon_r$ and size-effect-free characteristic are also achieved in

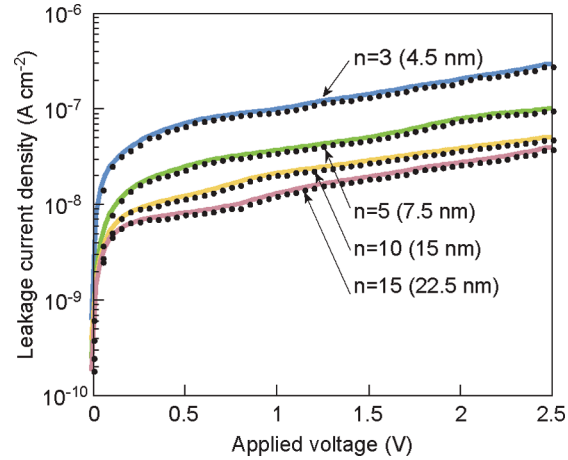


**Figure 6. $J-V$ curves of Au/$(Ca_2Nb_3O_{10})_n/SrRuO_3$.**

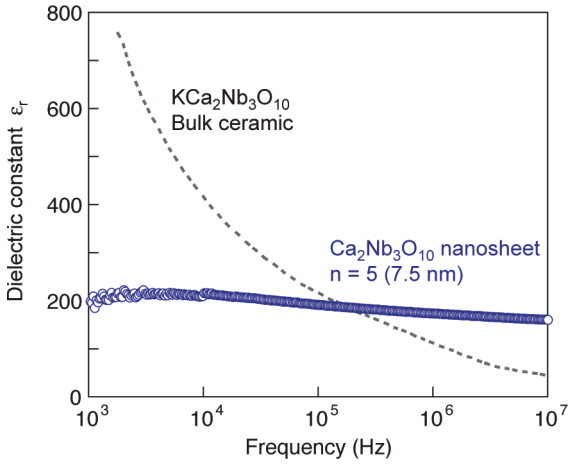


**Figure 7. Frequency dependence of $\varepsilon_r$ in a 7.5-nm-thick $(Ca_2Nb_3O_{10})_n$ ($n = 5$) film and $KCa_2Nb_3O_{10}$ bulk ceramic.**

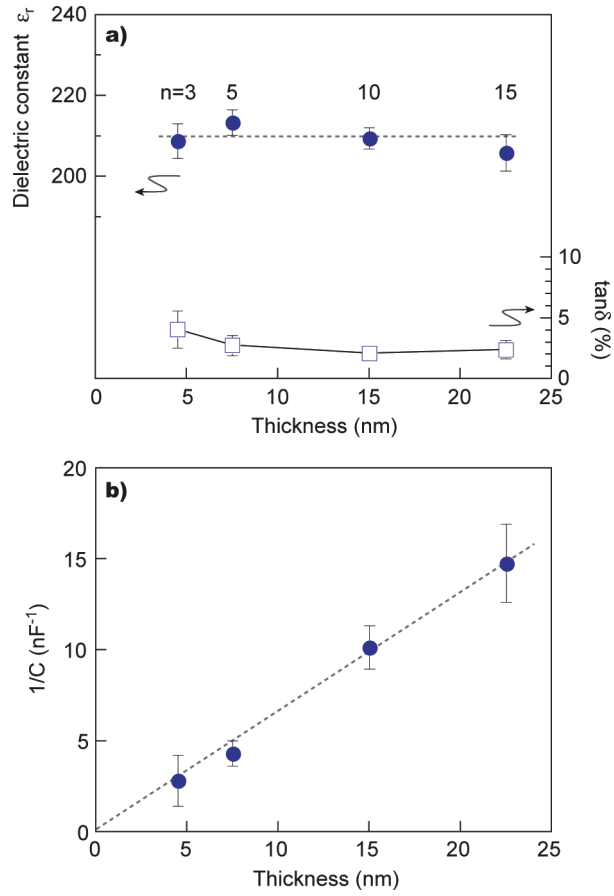


**Figure 8. (a) Variation of $\varepsilon_r$ and tan δ in multilayer $(Ca_2Nb_3O_{10})_n$ films as a function of film thickness. Dielectric measurement was performed at 100 kHz. (b) Thickness dependence of the reciprocal capacitance 1/*C* in multilayer $(Ca_2Nb_3O_{10})_n$ films.**

*A*- and *B*-site modified nanosheets ($Sr_2Nb_3O_{10}$, $Ca_2Ta_3O_{10}$, and $Sr_2Ta_3O_{10}$) (Figure 9a). It is noted that the optimized $\varepsilon_r$ value in a 9-nm-thick $Sr_2Nb_3O_{10}$ film reaches ~240, which is 10 times larger than that of $(Ba_{1-x}Sr_x)TiO_3$ films with the same thickness. In this context, we investigated electronic permittivity by first-principles calculations using the CASTEP package within the density-functional theory (see Methods).[29,30] We find that perovskite nanosheets exhibit high electronic permittivity, and the calculated electronic permittivity scales well with the observed $\varepsilon_r$ values (inset in Figure 9a). This relationship in perovskite nanosheets is a peculiar feature related to their large molecular polarizability, and the high-κ properties are materials properties inherent to perovskite nanosheets. In Figure 9b, we summarize the maximum values of $\varepsilon_r$ for perovskite nanosheets as well as various perovskite thin films[7−12,31−33] for comparison. In the ultrathin region (<20 nm), the $\varepsilon_r$ values of Nb-based perovskite nanosheets are larger than those of the other perovskites. The high $\varepsilon_r$ values of perovskite nanosheets persist even in the <10 nm region, which is in sharp contrast to a size-induced dielectric collapse in $(Ba_{1-x}Sr_x)TiO_3$.[7−12] These results suggest that perovskite nanosheets are a very promising candidate for high-density capacitor applications.

A clear benefit of our approach is the experimental realization of the atomically sharp interface between high-κ perovskites and electrodes. One of the most perplexing aspects of perovskite thin films is the origin of the interfacial low-κ dead layer. Current film growth techniques inevitably cause competing effects including incomplete screening at the electrode (intrinsic effects) and processing issues such as defects and strains (extrinsic effects); the dead-layer effect complicates the behavior. In our case, the multilayer nanosheets are a rather clean system without degradation of the interface and thermal strain, which could eliminate the extrinsic origin arising from the electrodes.

We can now gain further insight into the dead-layer effects by separating the intrinsic and extrinsic contributions. Recent *ab initio* studies[15] on high-κ capacitors suggest the incomplete screening at the electrode as the main cause of the intrinsic dead-layer effect; improved screening properties (using Pt electrodes with shorter electronic screening length) are crucial to reducing the dead layer. To check this conjecture, we carried out experiments using Pt/$(Ca_2Nb_3O_{10})_n$/Pt capacitors, and obtained $\varepsilon_r = 210 - 224$, similar to the Au/$(Ca_2Nb_3O_{10})_n$/$SrRuO_3$ case (Figures S1, S2, Supporting Information). It is interesting to note that many experiments on $(Ba_{1-x}Sr_x)TiO_3$ thin films have reported a different trend, that is, the pronounced dead-layer-induced reduction in the $\varepsilon_r$ value observed in Pt compared to that in $SrRuO_3$.[12] These results suggest that the extrinsic effects arising from growth-induced defects and strains have a dominant role in determining the observed dielectric properties of $(Ba_{1-x}Sr_x)TiO_3$/Pt devices, while in our nanosheet capacitors the superior interface quality brings improved screening properties, yielding a measured κ close to the bulk value. We also note that the size-free high-κ characteristic observed in our nanosheets is not specific to material choice and interface geometry. Recent experiments on $Ti_{0.87}O_2$ nanosheet show a size-

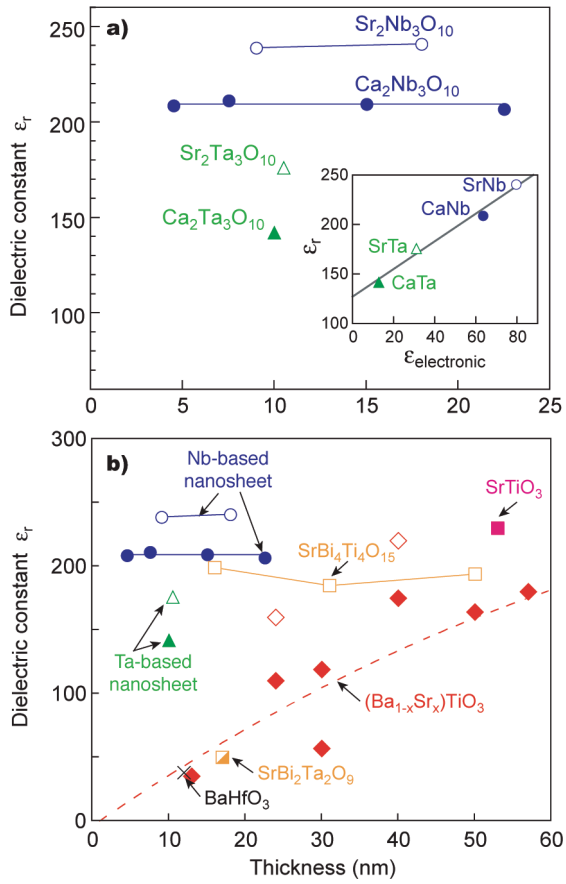


**Figure 9. (a) Variation of $\varepsilon_r$ in multilayer films of perovskite nanosheets. (Inset) Relationship between the observed $\varepsilon_r$ and calculated electronic permittivity in perovskite nanosheets. Electronic permittivity was also investigated by first-principles calculations within the density-functional theory. (b) Maximum values of $\varepsilon_r$ for perovskite nanosheets, as well as various perovskite thin films. Circles and triangles show perovskite nanosheets in the present study [$Ca_2Nb_3O_{10}$ (●), $Sr_2Nb_3O_{10}$ (○), $Ca_2Ta_3O_{10}$ (▲), and $Sr_2Ta_3O_{10}$ (Δ)]. Data for $Ba_{0.7}Sr_{0.3}TiO_3$ (ref 8) (◇), $Ba_{0.5}Sr_{0.5}TiO_3$ (refs 9−12) (◆), $SrTiO_3$ (ref 31) (■), $SrBi_4Ti_4O_{15}$ (ref 32) (□), $SrBi_2Ta_2O_9$ (ref 32) (◪), and $BaHfO_3$ (ref 33) ( ×) are also included for comparison.**

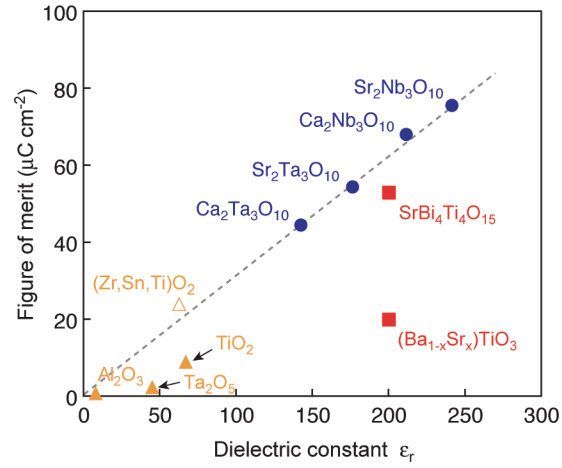


**Figure 10. Figure-of-merit values for perovskite nanosheets as well as various high-κ thin films. Data for $Zr_{0.15}Sn_{0.3}Ti_{0.55}O_{2-d}$ (ref 35), $TiO_2$ (ref 36), $Ta_2O_5$ (ref 37), $(Ba_{1-x}Sr_x)TiO_3$ (ref 7), and $SrBi_4Ti_4O_{15}$ (ref 32) are also included for comparison. The dotted line is a guide for the eye.**

effect-free high-κ characteristic ($\varepsilon_r$ = ~120) on a $SrRuO_3$ electrode,[34] in qualitative agreement with perovskite nanosheets. We thus conclude that in our nanosheets, the incomplete screening at the electrode has a minor role even in the $SrRuO_3$ case. The highly polarizable nature of perovskite nanosheets might compensate for the relatively inefficient electronic screening capabilities in $SrRuO_3$, and thus possibly eliminate any dead-layer effect at the interface.

These results are of major technological importance to achieve key nanoscale capacitor components in high-κ devices. In real capacitors, the overall dielectric performance is determined by both the permittivity and the leakage current. A useful figure of merit (FOM) can be defined as the product of these parameters, that is, FOM = $CV_{br}/S$, where $V_{br}$ is the maximum working voltage and $S$ is the area of electrodes.[35] As $C = \varepsilon_0\varepsilon_r S/d$ and $V_{br} = E_{br}d$, where $d$ is the dielectric thickness, $\varepsilon_0$ is the permittivty of free space, and $E_{br}$ is the breakdown field, FOM can also be defined as FOM = $\varepsilon_r E_{br}$ that corresponds to the maximum charge storage on a capacitor. Figure 10 summarizes the FOM values for perovskie nanosheets as well as various high-κ thin films. Clearly, perovskite nanosheets afford high capacitances with a dependence on high-κ values and molecularly thin thickness $d$, thus allowing for efficient charge storage and meanwhile reducing leakage currents. It should be also noted that perovskite nanosheets are of a paraelectric ground, thus yielding a very small temperature coefficient ($\tau$) of the capacitance (−150 to +80 ppm/°C) between −50 and 200 °C. The simultaneous improvements of $\varepsilon_r$, $\tau$, and $J$ properties in the ultrathin forms of single-phase materials are desirable for many applications, and the outstanding properties of the self-assembled dielectrics may open the way to new and improved devices far beyond the conventional top-down processes.

## CONCLUSIONS

We have demonstrated a rational approach for building high-κ nanodielectrics using the bottom-up assembly of perovskite nanosheets. The success of growth of nanofilms with a good interface quality enabled us to realize full potential high-κ dielectric properties of perovskite nanosheets, while eliminating the size effect encountered in current film-growth techniques. The nanofilms of $(Ca,Sr)_2Nb_3O_{10}$ nanosheets exhibit high dielectric constant (>200), the largest value seen so far in perovskite films with the thickness down to 10 nm. Furthermore, the superior high-κ properties are a size-effect-free characteristic with low leakage current density (<$10^{-7}$ A cm$^{-2}$). These results are of major technological importance to achieve key nanoscale capacitor components in high-κ devices. In capacitor components, high-κ and low tan δ are important crite-

ria for designing miniaturized and elegant devices, but it is no less important that the manufactured components exhibit constant fidelity over a wide range of operational conditions (such as frequency and temperature) with low leakage current density. In this context, perovskite nanosheets afford robust high-κ responses in molecularly thin thicknesses, thus allowing for efficient charge storage and meanwhile reducing leakage currents. Furthermore, the simultaneous improvements of $\varepsilon_r$, τ, and *J* properties in the ultrathin forms of single-phase materials are desirable for practical high-κ devices. The solution-based room-temperature process using nanosheets as building blocks opens multiple possibilities for deployment of high-κ dielectrics in integrated circuit technology, gate insulators in organic field-effect transistors, energy storage devices, and also future materials technologies, such as multiferroics and future flexible electronics.

## METHODS

**Synthesis of Nanosheet.** Perovskite nanosheets were prepared by delaminating layered perovskites according to previously described procedures.[22,23] The starting material $KCa_2Nb_3O_{10}$, prepared by a solid-state reaction, was converted into a protonic form, $HCa_2Nb_3O_{10} \cdot 1.5H_2O$, in $HNO_3$ solution. A colloidal suspension of $Ca_2Nb_3O_{10}$ nanosheets was synthesized by delaminating $HCa_2Nb_3O_{10} \cdot 1.5H_2O$, with tetrabutylammonium hydroxide solution (TBAOH). $Sr_2Nb_3O_{10}$, $Ca_2Ta_3O_{10}$, and $Sr_2Ta_3O_{10}$ nanosheets were also synthesized by delaminating layered perovskites ($KSr_2Nb_3O_{10}$, $KCa_2Ta_3O_{10}$, and $KSr_2Ta_3O_{10}$).

**Film Fabricaion.** The multilayered films were fabricated by layer-by-layer assembly using the LB process. An atomically flat conducting $SrRuO_3$ substrate, consisting of a 50-nm-thick (001)-oriented epitaxial $SrRuO_3$ film on a (001) $SrTiO_3$ single crystal, was used as a substrate. Before the film deposition, the substrate ($1 \times 1$ cm$^2$) was photochemically cleaned using UV light irradiation in ozone. Highly organized monolayer films were then fabricated by the LB process, as described in detail elsewhere (refs 25 and 26). A diluted colloidal suspension (*ca.* 0.032 g dm$^{-3}$) of the nanosheets was used as a subphase to form LB films without amphiphilic molecules. During LB deposition, the packing density of the nanosheets in the film could be controlled by the surface pressure of the air−water interface. The procedure for the LB depositions was repeated an appropriate number of times to synthesize a multilayer assembly composed of *n* layers. These films were irradiated by UV white light from a Xe lamp (1 mW cm$^{-2}$) for 24 h in order to decompose $TBA^+$ ions used in the exfoliation process.

**Characterization.** The film quality of the multilayer nanofilms was characterized by HRTEM, AFM, and XRD. Cross-sectional HRTEM was carried out using a Hitachi H-9000 microscope operating at 200 kV, which has a point resolution of 0.1 nm. Film surface morphology was analyzed using an SII Nanotechnology E-Sweep AFM. XRD patterns were collected by a Rigaku RINT 2200 diffractometer using monochromatized Cu Kα radiation (λ = 0.15405 nm).

**Electrical Characterization.** Electrical measurement was carried out by forming Au/(nanosheet)$_n$/$SrRuO_3$ capacitors. Au top-electrodes (50-nm-thick, 100 μm diameter) were deposited using the vacuum evaporation method. Different capacitors (with size electrodes of $10 \times 10$, $50 \times 50$, and $100 \times 100$ μm$^2$) were also investigated to check the possible effects of the lateral size and edges on dielectrics properties. Capacitance and dielectric loss tan δ were measured using a precision impedance analyzer (Agilent Technologies 4294A) in the range of 50 Hz−10 MHz. Leakage current properties were measured using a semiconductor parameter analyzer (Keithley 4200-SCS). Complementally data were obtained from Pt/(nanosheet)$_n$/Pt capacitors where a 25-nm-thick Pt film on a (001) $SrTiO_3$ single crystal was used as a substrate (Supporting Information, Figures S1, S2).

**First-Principles Calculations.** Electronic permittivity was investigated by first-principles calculations using the CASTEP package within the density-functional theory.[29,30] We used norm-conserving pseudopotentials. Oxygen 2s and 2p electrons, Ca 3s, 3p, and 4s electrons, Sr 4s, 4p, and 5s electrons, Nb 4s, 4p, and 5s electrons, and Ta 5d and 6s electrons were treated as valence states. The wave function was expanded in plane waves up to a kinetic energy cutoff of 500 eV. The Brillouin-zone sampling was performed by using a Monkhorst−Pack grid with a (3,6,1) grid of *k* points for a single-layered nanosheet. Structural optimizations were converged to a displacement of less than 0.0001 nm and an energy difference of less than $1 \times 10^{-5}$ eV/atom. Dielectric functions were calculated within the electric-dipole approximation.

*Acknowledgment.* This work was in part supported by World Premier International Research Center Initiative on Materials Nanoarchitronics, MEXT, Japan. M.O. acknowledges support from the Industrial Technology Research Grant Program (06A22702d), NEDO, and the Grant-in-Aid for Scientific Research (208591), MEXT, Japan.

*Supporting Information Available:* Additional figures. This material is available free of charge *via* the Internet at http://pubs.acs.org.

## REFERENCES AND NOTES

1. Scott, J. F. High-Dielectric Constant Thin Films for Dynamic Random Access Memories (DRAM). *Annu. Rev. Mater. Sci.* **1998**, *28*, 79–100.
2. Kingon, A. I.; Maria, J. P.; Streiffer, S. K. Alternative Dielectrics to Silicon Dioxide for Memory and Logic Devices. *Nature* **2000**, *406*, 1032–1038.
3. Ezhilvalavan, S.; Tseng, T. Y. Progress in the Developments of (Ba, Sr)$TiO_3$ (BST) Thin Films for Gigabit Era DRAMs. *Mater. Chem. Phys.* **2000**, *65*, 227–248.
4. Dawber, M.; Rabe, K. M.; Scott, J. F. Physics of Thin-Film Ferroelectric Oxides. *Rev. Mod. Phys.* **2005**, *77*, 1083–1130.
5. The latest edition of the ITRS roadmap can be found at http://public.itrs.net.
6. Kittl, J. A.; Opsomer, K.; Popovici, M.; Menou, N.; Kaczer, B.; Wang, X. P.; Adelmann, C.; Pawlak, M. A.; Tomida, K.; Rothschild, A.; *et al.* High-*k* Dielectrics and Metal Gates for Future Generation Memory Devices. *ECS Trans.* **2009**, *19*, 29–40.
7. Hwang, C. S.; Park, S. O.; Cho, H.-J.; Kang, C. S.; Kang, H. K.; Lee, S. I.; Lee, M. Y. Deposition of Extremely Thin (Ba, Sr)$TiO_3$ Thin Films for Ultra-Large-Scale Integrated Dynamic Random Access Memory Application. *Appl. Phys. Lett.* **1995**, *67*, 2819–2821.
8. Streiffer, S. K.; Basceri, C.; Parker, C. B.; Lash, S. E.; Kingon, A. I. Ferroelectricity in Thin Films: The Dielectric Response of Fiber-Textured $(Ba_xSr_{1-x})Ti_{1+y}O_{3+z}$ Thin Films Grown by Chemical Vapor Deposition. *J. Appl. Phys.* **1999**, *86*, 4565–4575.
9. Padmini, P.; Taylor, T. R.; Lefevre, M. J.; Nagra, A. S.; York, R. A.; Speck, J. S. Realization of High Tunability Barium Strontium Titanate Thin Films by *Rf* Magnetron Sputtering. *Appl. Phys. Lett.* **1999**, *75*, 3186–3188.
10. Werner, M. C.; Banerjee, I.; McIntyre, P. C.; Tani, N.; Tanimura, M. Microstructure of (Ba, Sr)$TiO_3$ Thin Films Deposited by Physical Vapor Deposition at 480 °C and Its Influence on the Dielectric Properties. *Appl. Phys. Lett.* **2000**, *77*, 1209–1211.
11. Craciun, V.; Singh, R. K. Characteristics of the Surface Layer of Barium Strontium Titanate Thin Films Deposited by Laser Ablation. *Appl. Phys. Lett.* **2000**, *76*, 1932–1934.

12. Hwang, C. S. Thickness-Dependent Dielectric Constant of (Ba, Sr)$TiO_3$ Thin Films with Pt or Conducting Oxide Electrodes. *J. Appl. Phys.* **2002**, *92*, 432–437.
13. Sinnamon, L. J.; Saad, M. M.; Bowman, R. M.; Gregg, J. M. Exploring Grain Size as a Cause for Dead-Layer Effects in Thin Film Capacitors. *Appl. Phys. Lett.* **2002**, *81*, 703–705.
14. Mead, C. A. Anomalous Capacitance of Thin Dielectric Structures. *Phys. Rev. Lett.* **1961**, *6*, 545–546.
15. Stengel, M.; Spaldin, N. A. Origin of the Dielectric Dead Layer in Nanoscale Capacitors. *Nature* **2006**, *443*, 679–682.
16. Stengel, M.; Vanderbilt, D.; Spaldin, N. A. Enhancement of Ferroelectricity at Metal-Oxide Interfaces. *Nat. Mater.* **2009**, *8*, 392–397.
17. Chang, L. W.; Alexe, M.; Scott, J. F.; Gregg, J. M. Settling the "Dead Layer" Debate in Nanoscale Capacitors. *Adv. Mater.* **2009**, *21*, 4911–4914.
18. Zhou, C.; Newns, D. M. Intrinsic Dead Layer Effect and the Performance of Ferroelectric Thin Film Capacitors. *J. Appl. Phys.* **1997**, *82*, 3081–3088.
19. Natori, K.; Otani, D.; Sano, N. Thickness Dependence of the Effective Dielectric Constant in a Thin Film Capacitor. *Appl. Phys. Lett.* **1998**, *73*, 632–634.
20. Pertsev, N. A.; Zembilgotov, A. G.; Tagantsev, A. K. Effect of Mechanical Boundary Conditions on Phase Diagrams of Epitaxial Ferroelectric Thin Films. *Phys. Rev. Lett.* **1998**, *80*, 1988–1991.
21. Black, C. T.; Welser, J. J. Electric-Field Penetration into Metals: Consequences for High-Dielectric Constant Capacitors. *IEEE Trans. Electron Dev.* **1999**, *46*, 776–780.
22. Schaak, R. E.; Mallouk, T. E. Perovskites by Design: A Toolbox of Solid-State Reactions. *Chem. Mater.* **2002**, *14*, 1455–1471.
23. Ebina, Y.; Sasaki, T.; Watanabe, M. Study on Exfoliation of Layered Perovskite-Type Niobates. *Solid State Ionics* **2002**, *151*, 177–182.
24. Shannon, R. D. Dielectric Polarizabilities of Ions in Oxides and Fluorides. *J. Appl. Phys.* **1993**, *73*, 348–366.
25. Muramatsu, M.; Akatsuka, K.; Ebina, Y.; Wang, K.; Sasaki, T.; Ishida, T.; Miyake, K.; Haga, M. Fabrication of Densely Packed Titania Nanosheet Films on Solid Surface by Use of Langmuir−Blodgett Deposition Method without Amphiphilic Additives. *Langmuir* **2005**, *21*, 6590–6595, 2005.
26. Akatsuka, K.; Haga, M.; Ebina, Y.; Osada, M.; Fukuda, K.; Sasaki, T. Construction of Highly Ordered Lamellar Nanostructures through Langmuir−Blodgett Deposition of Molecularly Thin Titania Nanosheets Tens of Micrometers Wide and Their Excellent Dielectric Properties. *ACS Nano* **2009**, *3*, 1097–1106.
27. Fang, M.; Kim, C. H.; Mallouk, T. E. Dielectric Properties of the Lamellar Niobates and Titanoniobates $AM_2Nb_3O_{10}$ and $ATiNbO_5$ (A = H, K, M = Ca, Pb), and Their Condensation Products $Ca_4Nb_6O_{19}$ and $Ti_2Nb_2O_9$. *Chem. Mater.* **1999**, *11*, 1519–1525.
28. Li, B. W.; Osada, M.; Ebina, Y.; Ozawa, T. C.; Ma, M.; Sasaki, T. Impact of Perovskite Layer Stacking on Dielectric Responses in $KCa_2Na_{n-3}Nb_nO_{3n+1}$ (n = 3−6) Dion−Jacobson Homologous Series. *Appl. Phys. Lett.* **2010**, *96*, 182903−1–3.
29. Segall, M. D.; Lindan, P. J. D.; Probert, M. J.; Pickard, C. J.; Hasnip, P. J.; Clark, S. J.; Payne, M. C. First-Principles Simulation: Ideas, Illustrations and the CASTEP Code. *J. Phys.: Condens. Matter* **2002**, *14*, 2717–2744.
30. Sato, H.; Ono, K.; Sasaki, T.; Yamagishi, A. First-Principles Study of Two-Dimensional Titanium Dioxides. *J. Phys. Chem. B* **2003**, *107*, 9824–9828.
31. Abe, K.; Komatsu, S. Epitaxial Growth of $SrTiO_3$ Films on Pt Electrodes and Their Electrical Properties. *Jpn. J. Appl. Phys.* **1992**, *31*, 2985–2988.
32. Takahashi, K.; Suzuki, M.; Kojima, T.; Watanabe, T.; Sakashita, Y.; Kato, K.; Sakata, O.; Sumitani, K.; Funakubo, H. Thickness Dependence of Dielectric Properties in Bismuth-Layer-Structured Dielectrics. *Appl. Phys. Lett.* **2006**, *89*, 082901−1−3.
33. Lupina, G.; Kozłowski, G.; Dabrowski, J.; Wenger, Ch.; Dudek, P.; Zaumseil, P.; Lippert, G.; Walczyk, Ch.; Müssig, H. J. Thin $BaHfO_3$ High-*k* Dielectric Layers on TiN for Memory Capacitor Applications. *Appl. Phys. Lett.* **2008**, *92*, 062906−1−3.
34. Osada, M.; Ebina, Y; Funakubo, H.; Yokoyama, S.; Kiguchi, T.; Takada, K.; Sasaki, T. High-*k* Dielectric Nanofilms Fabricated from Titania Nanosheets. *Adv. Mater.* **2006**, *18*, 1023–1026.
35. van Dover, R. B.; Schneemeyer, L. F.; Fleming, R. M. Discovery of a Useful Thin-Film Dielectric Using a Composition-Spread Approach. *Nature* **1998**, *392*, 162–164.
36. Kim, S. K.; Kim, W.-D.; Kim, K.-M.; Hwang, C.-S.; Jeong, J. High Dielectric Constant $TiO_2$ Thin Films on a Ru Electrode Grown at 250 °C by Atomic-Layer Deposition. *Appl. Phys. Lett.* **2004**, *85*, 4112–4114.
37. Kukli, K.; Ritala, M.; Leskelä, M. Development of Dielectric Properties of Niobium Oxide, Tantalum Oxide and Alminum Oxide Based on Nanolayered Materials. *J. Electrochem. Soc.* **2001**, *148*, F35–F41.